The Astronomical Journal, 172:183 (13pp), 2026 September https://doi.org/10.3847/1538-3881/ae8bb0
© 2026. The Author(s). Published by the American Astronomical Society.
OPEN ACCESS

The Occurrence Rate of Nearby Planetary Companions to Hot Jupiters

Lizhou Sha[1], Andrew M. Vanderburg[2], Chelsea X. Huang[3,26], Samuel Christian[4], Kevin Burdge[4], Nicholas Saunders[5,6], Khalid Barkaoui[7,8,9], Alexander Belinski[10], Serge Bergeron[11,12], Zoë L. de Beurs[13,27], Allyson Bieryla[2], Karen A. Collins[2], Giuseppe Conzo[14], Gareb Fernández-Rodríguez[7,15], Akihiko Fukui[7,16], Davide Gandolfi[17], Tristan Guillot[18], Joel D. Hartman[1], Kai Ikuta[19], David W. Latham[2], Jerome P. de Leon[16], Bob Massey[12], Gabriel Murawski[20], Felipe Murgas[7,15], Norio Narita[7,16,21], Mohammad Odeh[22], Enric Palle[7,15], Hannu Parviainen[7,15,28], Gabrielle Ross[1], Richard P. Schwarz[2], Gregor Srdoc[23], Chris Stockdale[24], Samuel N. Quinn[2], Ian A. Waite[3], Francis P. Wilkin[25], and George Zhou[3,26]

[1] Department of Astrophysical Sciences, Princeton University, 4 Ivy Lane, Princeton, NJ 08540, USA
[2] Center for Astrophysics|Harvard & Smithsonian, 60 Garden Street, Cambridge, MA 02138, USA
[3] Centre for Astrophysics, University of Southern Queensland, Toowoomba, QLD 4350, Australia
[4] Department of Physics and Kavli Institute for Astrophysics and Space Research, Massachusetts Institute of Technology, 77 Massachusetts Avenue, Cambridge, MA 02139, USA
[5] Department of Astronomy, Yale University, New Haven, CT 06511, USA
[6] Institute for Astronomy, University of Hawaii at Mānoa, 2680 Woodlawn Drive, Honolulu, HI 96822, USA
[7] Instituto de Astrofisica de Canarias (IAC), E-38200 La Laguna, Tenerife, Spain
[8] Astrobiology Research Unit, Université de Liège, Allée du 6 Août 19C, B-4000 Liège, Belgium
[9] Department of Earth, Atmospheric and Planetary Science, Massachusetts Institute of Technology, 77 Massachusetts Avenue, Cambridge, MA 02139, USA
[10] Sternberg Astronomical Institute, Lomonosov Moscow State University, Universitetskii prospekt, 13, Moscow 119992, Russia
[11] American Public University, USA
[12] American Association of Variable Star Observers, 185 Alewife Brook Parkway Suite 410, Cambridge, MA 02138, USA
[13] Department of Earth, Atmospheric and Planetary Sciences, Massachusetts Institute of Technology, Cambridge, MA 02139, USA
[14] Gruppo Astrofili Palidoro, Italy
[15] Departamento de Astrofisica, Universidad de La Laguna (ULL), E-38206 La Laguna, Tenerife, Spain
[16] Komaba Institute for Science, The University of Tokyo, 3-8-1 Komaba, Meguro, Tokyo 153-8902, Japan
[17] Dipartimento di Fisica, Università degli Studi di Torino, via Pietro Giuria 1, 10125, Torino, Italy
[18] Observatoire de la Côte d'Azur, Université Côte d'Azur, CNRS, Laboratoire Lagrange, Bd de l'Observatoire, CS 34229, 06304, Nice cedex 4, France
[19] Department of Social Data Science, Hitotsubashi University, 2-1 Naka, Kunitachi, Tokyo 186-8601, Japan
[20] Gabriel Murawski Private Observatory (SOTES), Poland
[21] Astrobiology Center, 2-21-1 Osawa, Mitaka, Tokyo 181-8588, Japan
[22] International Astronomical Center, 45015, Abu Dhabi, UAE
[23] Kotizarovci Observatory, Sarsoni 90, 51216 Viskovo, Croatia
[24] Hazelwood Observatory, Australia
[25] Union College, Schenectady, NY 12308, USA
Received 2025 October 3; revised 2026 June 15; accepted 2026 June 18; published 2026 August 31

Abstract

Of the >500 confirmed transiting hot Jupiters and ≈2000 additional candidates today, only 10 are known to have nearby companion planets. The survival of nearby companions means that these hot Jupiters cannot have migrated to their present location via dynamically disruptive high-eccentricity migration but instead have undergone disk migration or formed in situ. The occurrence rate for these nearby companions, therefore, constrains the relative efficiency of different hot Jupiter formation pathways. Here, we perform a uniform box least-squares search for nearby transiting companions to hot Jupiters in the first 5 yr of TESS data. Accounting for observational completeness and detection efficiency, we arrive at an occurrence rate of $(7.6^{+5.5}_{-3.8})\%$, which is a lower limit on the fraction of hot Jupiters that underwent disk migration or in situ formation. Comparing this rate with that derived from transit-timing variation searches suggests that hot Jupiters are likely mostly aligned with their nearby companions, but their apparently higher incidence of grazing transits may point to a slight preferential misalignment. We also synthesize evidence that hot Jupiters with nearby companions may have cold companions at a rate similar to that of other hot Jupiters. Comprehensive transit, radial velocity, and stellar obliquity measurements in hot Jupiter systems with nearby companions will be necessary to fully account for the relative prevalence of proposed hot Jupiter formation pathways.

Unified Astronomy Thesaurus concepts: Hot Jupiters (753); Exoplanet systems (484); Transit photometry (1709); Exoplanet migration (2205)

Materials only available in the online version of record: machine-readable table

1. Introduction

The existence of nearby planetary companions to hot Jupiters in the present is a powerful diagnostic of their formation in the past. Although hot Jupiters, or gas giant planets with orbital periods less than 10 days, were among the first exoplanets ever discovered, we have yet to complete the theoretical accounting of their formation. Under the core

[26] ARC Future Fellow.
[27] NSF Graduate Research Fellow, MIT Presidential Fellow, MIT Collamore-Rogers Fellow.
[28] Ramón y Cajal Fellow.

Original content from this work may be used under the terms of the Creative Commons Attribution 4.0 licence. Any further distribution of this work must maintain attribution to the author(s) and the title of the work, journal citation and DOI.

accretion paradigm (e.g., J. B. Pollack et al. 1996), gas giant planets like Jupiter and Saturn should only form at large orbital separations from their host stars, beyond "snow lines" where volatile materials exist in solid form within the protoplanetary disk. The discovery of the prototypical hot Jupiter 51 Peg b (M. Mayor & D. Queloz 1995), therefore, initially came as a surprise. While an alternative is for hot Jupiters to form in situ near where they are found today after being seeded by super-Earth-sized planets (K. Batygin et al. 2016), a majority of the literature resolves this apparent conflict by proposing that they formed "cold" via core accretion and then migrated to their present "hot" location. Whether nearby planetary companions to hot Jupiters can exist depends on how this migration unfolds.

Two main migration pathways have been proposed for hot Jupiters: high-eccentricity (or tidal) migration (e.g., F. A. Rasio & E. B. Ford 1996) and disk migration (e.g., D. N. C. Lin et al. 1996). Under high-eccentricity migration (HEM), a Jupiter-sized planet that formed beyond the snow line is perturbed into a highly eccentric orbit by gravitational interactions with an outer planetary or stellar companion. From there, tides raised on the planet during periastron passage gradually dissipate its orbital energy and shrink its semimajor axis until its orbit circularizes. Under disk migration, on the other hand, the hot Jupiter forms before the protoplanetary disk completely dissipates and interacts with the disk to gradually reduce its orbital period. Understanding in what proportion these two migration pathways (along with in situ formation) are responsible for the known population of hot Jupiters is a major goal of exoplanet science.

One way to discriminate these formation pathways is to look for smaller planets orbiting interior to hot Jupiters. Because HEM is dynamically disruptive, it is expected that no inner companion could have survived the process (A. J. Mustill et al. 2015). If an inner companion is found, we could all but eliminate HEM as a mechanism by which that hot Jupiter could have formed. Thus, studying the population of nearby planetary companions to hot Jupiters presents an opportunity to constrain the fraction of these systems that formed via dynamically quiet pathways.

Early estimates of the occurrence rate of nearby planetary companions to hot Jupiters were hampered by a limited sample of transiting hot Jupiters observed with sufficient photometric precision to detect small companion planets. For 20 yr after the discovery of 51 Peg b, no hot Jupiters were found to have nearby planetary companions (e.g., E. Miller-Ricci et al. 2008; J. H. Steffen et al. 2012), even while smaller planets were frequently found in multiplanet systems (D. W. Latham et al. 2011) by the Kepler prime mission. Subsequently, during the K2 mission, the discovery of nearby planetary companions to the hot Jupiter WASP-47 b (J. C. Becker et al. 2015) showed that at least some hot Jupiters form in a dynamically quiet manner, either via disk migration or in situ. This discovery prompted the first estimate of the occurrence rate of nearby companions to hot Jupiters ($1.1^{+13.3}_{-1.1}$%, median and 90% interval) by C. Huang et al. (2016), suggesting that those systems were rare, although this rate was based on null detection during the Kepler prime mission at the time. Similarly, after the discovery of Kepler-730 c by reanalysis of Kepler prime mission planet candidates (W. Zhu et al. 2018; C. I. Cañas et al. 2019), W. Zhu & S. Dong (2021) also made an independent estimate based on the final Kepler DR25 planet candidate catalog (S. E. Thompson et al. 2018), counting Kepler-730 as a detection, and arrived at a similar occurrence rate (≈2%, or <9.7% at a 95% upper limit) for nearby ($P \lesssim 20$ days), small (≈1–4 $R_\oplus$), and nearly coplanar companions to hot Jupiters.

The apparent loneliness of hot Jupiters suggests that HEM is likely the dominant formation pathway. Nevertheless, the relatively large uncertainty on the occurrence rate, a consequence of the relatively small number of hot Jupiters searched, limits the strength of conclusions about hot Jupiter formation that can be drawn. Thanks to its wide field of view, nearly full-sky coverage, and full-frame images with sufficient cadence, NASA's Transiting Exoplanet Survey Satellite (TESS) has brought a flood of hot Jupiter candidates. Hot Jupiters are intrinsically rare (J. T. Wright et al. 2012), and it is difficult to construct large statistical samples without this comprehensive sky coverage and high data volume. Before TESS, the best statistical sample of hot Jupiters was from the Kepler mission, but because Kepler was only able to downlink data for about 200,000 stars, it only detected 40–60 hot Jupiters from its primary mission (S. E. Thompson et al. 2018; S. W. Yee et al. 2021). TESS, on the other hand, observes and downlinks data for millions of stars bright enough for hot Jupiter detection each month. As a result, it has already observed thousands of hot Jupiters (N. M. Guerrero et al. 2021), the vast majority of which are new discoveries (e.g., J. E. Rodriguez et al. 2021, 2023; S. W. Yee et al. 2022, 2023; J. Schulte et al. 2024). This large number of discoveries, coupled with TESS's very high sensitivity to these planets (making large magnitude- and volume-limited samples nearly complete) and relatively unbiased target selection, has enabled important advancements in hot Jupiter population studies (e.g., G. Zhou et al. 2019; M. Beleznay & M. Kunimoto 2022; S. W. Yee & J. N. Winn 2023). Among these results was the measurement of the occurrence rate of nearby companions around hot Jupiters by B. J. Hord et al. (2021), who used a sample of about 179 hot Jupiters to determine that about $7.3^{+15.2}_{-7.3}$% (median and 90% interval, or <27.8% at a 95th percentile upper limit) of hot Jupiters have a nearby planetary companion.

Our work builds on the large sample of hot Jupiters observed by TESS and previous demographic studies of nearby companions to hot Jupiters. Since the work by B. J. Hord et al. (2021), several other hot Jupiter systems with nearby companions have been discovered (C. X. Huang et al. 2020a; B. J. Hord et al. 2022; G. Maciejewski et al. 2023; L. Sha et al. 2023; J. Korth et al. 2024; B. J. McKee et al. 2025; J. R. Livesey et al. 2026; S. N. Quinn et al. 2026). This means that, for the first time, there is an opportunity to measure the occurrence rate of these nearby companions based on positive detections and a large statistical sample of hot Jupiters. Figure 1 provides a "family portrait" of the architectures of these compact multiplanet hot Jupiter systems.

In this work, we perform the largest-ever uniform search for short-period transiting companions to transiting hot Jupiters and calculate the occurrence rate of these companions corrected for observational biases and detection completeness, for the first time based on a positive number of detections. We identify ≈2000 likely hot Jupiters from the TESS Objects of Interest (TOI) catalog of planet candidates (Section 2). After

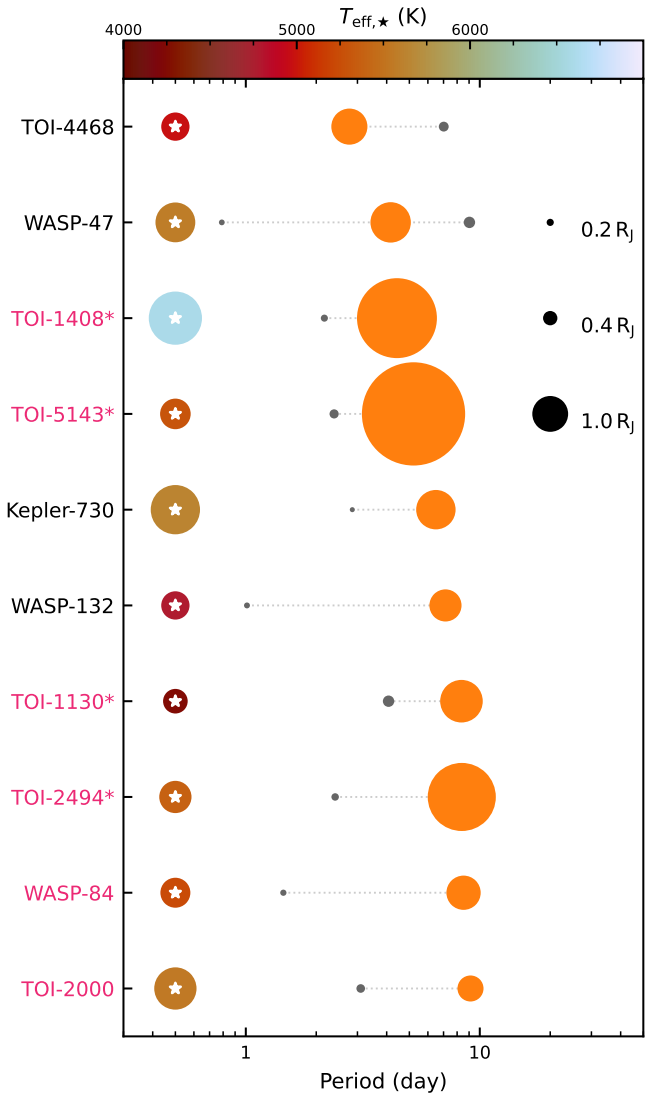


Figure 1. Transiting planetary systems hosting nearby planetary companions to hot Jupiters ($P < 10$ days). Nontransiting planets are omitted. The leftmost circle in each row represents the host star, with the mark's size indicating the stellar radius and color the stellar effective temperature (from TICv8; K. G. Stassun et al. 2019). The other circles represent the transiting planets in each system, with their sizes proportional to planet radii and colors indicating a giant planet (orange) or a small planet (gray). The relative mark sizes among either the stars or the planets are to scale, but those between a star and its planets are not. The translucent marks are planet candidates not yet published in the literature. Systems that are counted as detected (Section 4) for the occurrence rate calculation (Section 5) have their names highlighted in magenta, and systems whose giant planets have grazing transits (Section 6.3) are marked with an asterisk. The systems are sorted in ascending order of the period of the largest planet. This figure and its caption are adapted from Figure 10 of L. Sha et al. (2023), updated with newly available planetary parameters for the TOI-4468 (J. R. Livesey et al. 2026), TOI-2494, TOI-5143 (S. N. Quinn et al. 2026), and TOI-1408 (J. Korth et al. 2024) systems.

searching their light curves for transiting companions with small orbital periods (Section 3), we carefully vet any new signal and eliminate known astrophysical false positives such as eclipsing binaries or stellar variations, reporting our detections in Section 4. We characterize the sensitivity of our pipeline and calculate the occurrence rate for nearby companions, given the existence of these hot Jupiters (Section 5). We discuss the implications of the occurrence rate measurements and architectures of these planetary systems in Section 6, concluding with Section 7.

2. Sample of Hot Jupiters

We aimed to search every hot Jupiter observed during the first 5 yr (sectors 1–69) of the TESS mission for nearby planetary companions ($P < 10$ days). To that end, we assembled a list of confirmed and candidate hot Jupiters from the TOI (N. M. Guerrero et al. 2021) catalog. After carefully removing known or suspected nonplanets, we estimated the false-positive rate (FPR) of the remaining planet candidates on our list. Finally, we derived new stellar parameters from broadband photometry as the basis for the refined planetary parameters of the hot Jupiters. These procedures are detailed in the rest of this section.

2.1. Selecting Hot Jupiters

To start, we select TOI candidates

1. with valid Gaia DR2 cross-matches,
2. with periods $P < 10$ days,
3. with radii $8 \leqslant R_{\rm p}/R_{\oplus} < 30$ within uncertainty *and* measured to better than 50%, and
4. alerted on or before UT 2024 May 30

from the ExoFOP website (NExScI 2022, accessed on 2024 July 5). To identify TOI candidates that are known or suspected to not be planets, we eliminated targets with

1. unfavorable dispositions of the TESS Follow Up Program working group (TFOPWG)[29] from the ExoFOP website (accessed on 2025 March 11),
2. excess radial velocity (RV) scatter from Gaia DR3, and
3. $R_{\rm p} \geqslant 30\,R_{\oplus}$ and semimajor axis–to–stellar radius ratio $a/R_{\star} < 1$ based on the parameters derived in Section 2.3.

The TFOPWG dispositions are based on follow-up photometry, spectroscopy, and high-resolution imaging and identify TOI candidates that are known or suspected to be eclipsing binaries or other astrophysical false positives. The RV scatters from Gaia DR3 eliminate suspected spectroscopic binaries. We estimate the RV scatter $\sigma_{\rm RV}$ by multiplying the reported RV uncertainty (`radial_velocity_error`) and the square root of the number of RV observations (`rv_nb_transits`). Then, we use the following empirical formula based on the Gaia DR3 G magnitude to identify the targets with excess $\sigma_{\rm RV}$:

$$\frac{\sigma_{\rm RV}}{\rm km\ s^{-1}} > \begin{cases} 2 & G < 10, \\ 2 \cdot 10^{0.4(G-10)} & G \geqslant 10. \end{cases} \quad (1)$$

The TOI candidates that survive these checks comprise our sample of hot Jupiters searched for nearby companions, as long as their TESS light curve is available. They are tabulated in Table 1.

2.2. Estimation of False-positive Rate

In order to ensure the accuracy of our calculated occurrence rate (Section 5.4), we want to estimate the FPR, defined as the fraction of nonplanets, in our hot Jupiter sample. Starting from the original estimate for the FPR of TOIs from G. Zhou et al. (2019) based on 10 detected false positives among 31 TOIs, which we denote $\mathrm{FPR}_{\rm Zhou} = 10/31 \approx 0.32$, we expect to find

[29] Specifically, we eliminated planets designated as false positive (FP), false alert (FA), and ambiguous planetary candidates (APC) by the TFOPWG.

Table 1
Hot Jupiter Candidates from the TOI Catalog

TIC ID	Period (days)	Midtransit Time $BJD_{TDB} - 2457000$	Transit Depth	Duration (hr)	Stellar Mass ($M_\odot$)	Stellar Radius ($R_\odot$)	Planet Radius ($R_\oplus$)	$a/R_\star$	Impact Param.
4711	2.33481520	2358.079233	0.005310	1.86	1.202	1.432	11.4	5.499	0.912
56884	3.91748200	3088.668722	0.008397	2.62	1.322	1.574	15.7	7.292	0.890
160023	6.75655190	2358.443291	0.005200	3.44	1.214	1.622	12.8	9.893	0.847
857186	3.81236140	2465.891746	0.018330	2.56	0.826	0.788	11.6	12.227	0.365
1003831	1.65114558	1518.203428	0.003206	0.95	1.008	1.077	6.7	5.472	0.976
1129033	1.36002828	2168.520849	0.019428	2.17	0.982	1.045	15.9	4.913	0.526

Note. The first five columns are taken from the TOI catalog (N. M. Guerrero et al. 2021). The stellar masses and radii are from this work, and the last three columns are imputed from the values in the preceding columns assuming circular orbits (Section 2.3). These parameters are used in Section 5 to calculate observational completeness. While the values in this table are self-consistent and valid in the statistical aggregate, they should not be used in work demanding high accuracy in the context of individual planetary systems.

(This table is available in its entirety in machine-readable form in the online article.)

$\mathrm{FPR}_{\mathrm{Zhou}} \cdot N_{\mathrm{TOI}}$ false positives among the $N_{\mathrm{TOI}} = 2684$ TOIs that match our initial period, radius, and alert time criteria. We subsequently eliminated 570 confirmed or suspected nonplanets based on TFOPWG dispositions, 249 suspected spectroscopic binaries based on excess σ_{RV}, and 16 suspected nonplanets with implausible R_{p} or $a/R_\star$, for a combined total of $N_{\mathrm{FP}} = 749$. In theory, this elimination leaves us with

$$\mathrm{FPR}_{\mathrm{HJ}} = \frac{\mathrm{FPR}_{\mathrm{Zhou}} \cdot N_{\mathrm{TOI}} - N_{\mathrm{FP}}}{N_{\mathrm{TOI}} - N_{\mathrm{FP}}} \approx 0.060 \quad (2)$$

among the remaining 1935 hot Jupiters in our sample. This $\mathrm{FPR}_{\mathrm{HJ}}$ will be used in Section 5.4 to adjust the final effective sample size (ESS) of the hot Jupiters for the occurrence rate calculation.

2.3. Properties of the Hot Jupiters and Their Host Stars

In order to obtain more accurate planetary parameters, we derived masses and radii for the hot Jupiter host stars via spectral energy distribution (SED) fitting to Gaia DR3 G, G_{BP}, G_{RP} magnitudes and Two Micron All Sky Survey (2MASS) J, H, K magnitudes. We obtained these magnitudes by cross-matching the TESS Input Catalog version 8 (TICv8; K. G. Stassun et al. 2018, 2019) with the Gaia and 2MASS catalogs. (The targets that did not have Gaia DR2 cross-matches in TICv8 were not selected in the first place.) Given these broadband apparent magnitudes and Gaia DR3 parallaxes, we used the ISOCHRONES Python package (T. D. Morton 2015) to perform nested sampling of fundamental stellar parameters modeled by the MESA Isochrones and Stellar Tracks (MIST; J. Choi et al. 2016; A. Dotter 2016), using the associated correction tables to convert bolometric to broadband photometric magnitudes. To better reflect systematic and model uncertainty, we inflated the uncertainty for all measured magnitudes to 0.1.

The resulting new stellar masses $M_\star$ and radii $R_\star$, as well as derived planetary parameters, are tabulated in Table 1, and the distribution of stellar masses and the color–magnitude diagram are shown in Figure 2. We derived planet radii R_{p} from the new $R_\star$ and the transit depth from the TOI catalog and used the new $M_\star$ and $R_\star$ combined with the orbital period from the TOI catalog to calculate $a/R_\star$, which is then used in conjunction with our derived R_{p} and the transit duration from the TOI catalog to calculate the impact parameter b, assuming circular orbits. As mentioned in Section 2.1, we further identified all planets with $R_{\mathrm{p}} \geqslant 30\,R_\oplus$ and $a/R_\star < 1$ and eliminated them from the hot Jupiter sample as likely nonplanets. Since TOIs must be transiting, we clamped this derived b to the interval $[0, 1 + R_{\mathrm{p}}/R_\star)$. These new $M_\star$, $R_\star$ and derived R_{p}, b will be used to determine observational completeness for the occurrence rate calculation in Section 5.

3. Search for Additional Short-period Planets in Hot Jupiter Systems

To search for nearby transiting companions of hot Jupiters, we used light curves from the MIT Quick Look Pipeline (QLP) up to and including sector 69. Initially created for the TESS Prime Mission, QLP generates light curves for all targets in the TESS full-frame images (calibrated as described by M. M. Fausnaugh et al. 2020) brighter than a TESS magnitude of 13.5 and certain fainter targets with high proper motion (C. X. Huang et al. 2020b, 2020c; M. Kunimoto et al. 2021, 2022b). Since we perform detrending, or removal of the long-term variability in the light curves, as part of the planet search, we use the raw simple aperture photometry (`SAP_FLUX`) time series for light curves before sector 56 and the systematics-corrected (`SYS_RM_FLUX`) time series thereafter (M. Kunimoto et al. 2022a). There were 86 targets out of the 1935 hot Jupiter systems in our sample without valid QLP light curves, leaving us with $N_{\mathrm{HJ}} = 1849$ systems to be searched. We detail our planet search pipeline and candidate vetting procedures in this section.

3.1. Box Least-squares Search

We used the box least-squares (BLS; G. Kovács et al. 2002) algorithm to search for additional planets in the light curves of the hot Jupiters. After removing all points that have been flagged for quality issues (e.g., spacecraft anomaly, excess scattered light, etc.), we iteratively applied the following steps five times to each light curve.

1. Remove parts of the light curve containing hot Jupiter transits and signals corresponding to the previous peaks of the light curve.
2. Detrend the light curve, remove upward outliers, and estimate uncertainty.
3. Find the period and phase of the signal corresponding to the peak of the BLS power spectrum.

We detail these steps below.

Removal of known signals. We remove the hot Jupiter transits from the raw photometry light curve by masking points that lie within a span of 3 times the transit duration centered on

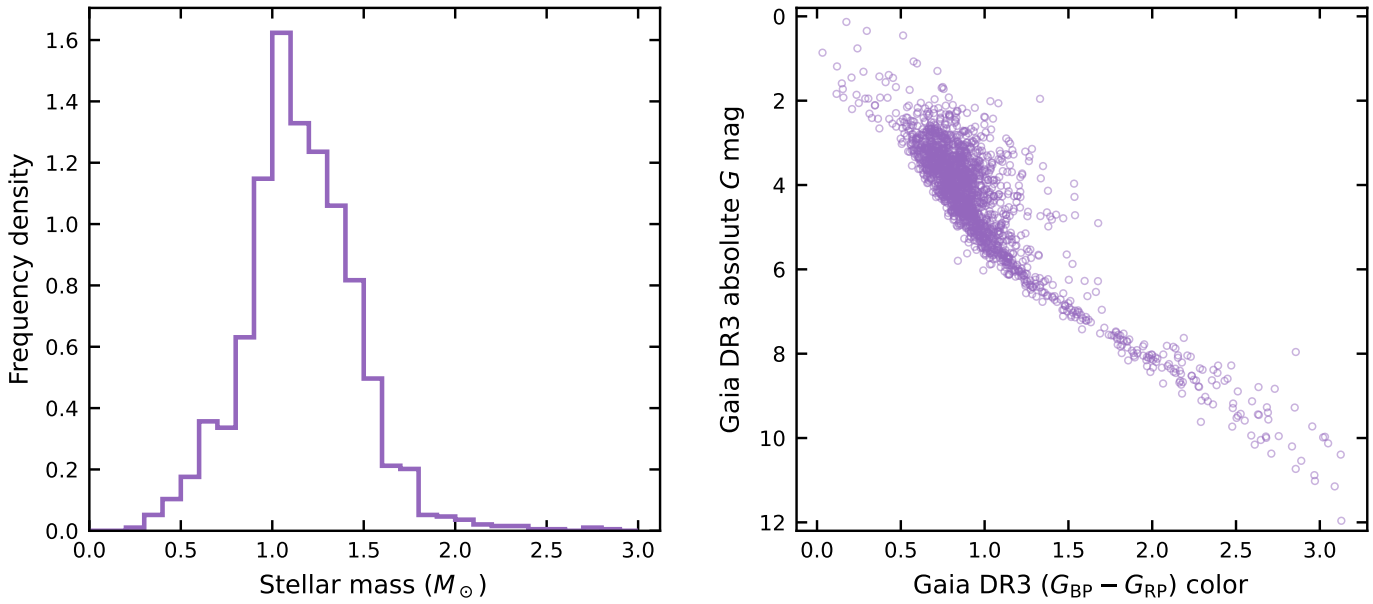


Figure 2. The distribution of the host stars of the selected hot Jupiters. Left: the histogram of stellar mass. Right: the color–magnitude diagram.

the midtransit time, with the transit ephemerides taken from the TOI catalog. In subsequent iterations, we also remove portions of the light curve corresponding to signals detected in previous iterations.

Detrending. We detrend the light curves using Keplerspline, a high-pass filtering method based on B-spline (A. Vanderburg & J. A. Johnson 2014; C. J. Shallue & A. Vanderburg 2018), in segments that are no more than approximately 14 days and also contain no gaps longer than 1 day. Keplerspline uses the Bayesian information criterion to automatically pick the most appropriate break-point spacing for each light curve. The detrended segments are then normalized and joined together to search for additional planets. Keplerspline estimates the standard deviation σ of the light curve from the median absolute deviation. This σ is calculated per sector and is used as the nominal uncertainty for all data points in a given sector for the subsequent transit search. We also reject points that lie more than 5σ above the spline in order to mitigate the effect of flares and instrumental artifacts on the transit detection algorithm.

Performing the BLS search. We use the CUVARBASE (J. Hoffman 2022) package for the BLS search, similar to QLP's implementation since sector 59 (M. Kunimoto et al. 2023). The CUVARBASE package uses the NVIDIA CUDA interface to implement BLS on the GPU. We search in the period range of 4 hr to 10 days with optimal frequency spacing $\delta f \propto f^{2/3}$ and a log-uniform grid of the transit duration fraction with 20 intervals between 2^{-7} and 2^{-2}. Since we use a fast implementation of BLS that only outputs the BLS power at each period, once we obtain the period with the highest BLS power, we use the ASTROPY package to obtain the transit parameters (midtransit time, transit duration $T_{\rm dur}$, and depth δ) at the detected period, following the methods implemented by VARTOOLS (J. D. Hartman & G. A. Bakos 2016). These parameters are used in subsequent iterations for signal removal.

3.2. Vetting Transit-like Signals

We declared any signal with a BLS signal-to-noise ratio S/N > 7 as computed by ASTROPY to be a threshold-crossing event (TCE), and all TCEs were vetted to ensure they are likely to be transiting planets. We applied the following criteria in order to automatically eliminate TCEs of low data quality or whose parameters are incompatible with being a planet:

1. number of points in transit $\geqslant$20;
2. number of transits (each with $\geqslant$3 points) $\geqslant$3;
3. $a/R_\star > 3$, where a is the semimajor axis and $R_\star$ is the stellar radius; and
4. $T_{\rm dur} < 3\,T_{\rm dur,circ}$, the transit duration assuming a circular orbit and impact parameter $b = 0$.

Both $a/R_\star$ and $T_{\rm dur,circ}$ were calculated from the stellar masses and radii from TICv8 and the period and transit depth of the TCE. All TCEs that fulfill these criteria, as well as TCEs whose stellar parameters are missing from TICv8, were retained for manual vetting.

We performed manual vetting in two distinct steps. In the first step, we generated three types of plots for each TCE: the BLS spectrum, the folded light curve centered on the TCE with binned points and the boxcar transit model, and undetrended light curves with the detrending spline and the transit signals highlighted. We used these plots to visually eliminate TCEs that

1. were not transit-like in shape,
2. showed significant odd–even variations, or
3. could be attributed to fast-varying portions of the light curve (e.g., scattered light near the beginning or end of an orbit) that the detrending step did not remove.

TCEs that survived the initial manual vetting were subject to additional scrutiny. We generated additional light curves with enhanced systematics correction from the full-frame images by extracting aperture photometry following A. Vanderburg et al. (2016) and correcting for spacecraft systematics using the procedures described by A. Vanderburg et al. (2019). These additional light curves were used to generate additional vetting plots, including a cutout view of the TESS full-frame image (FFI) and a simple pixel-level difference image of the median

in- and out-of-transit FFIs, with a customized version of the GIANTS package[30] (N. Saunders et al. 2022). Since TESS has a relatively large pixel size of 21″, the photometric aperture could enclose nearby targets that are blended or unresolved from the true target. Therefore, we also eliminated TCEs that showed a significant offset in the in- and out-of-transit difference image from the expected centroid of the target star. For the few TCEs that passed all previous vetting steps but were not known confirmed or candidate planets, we further used the TRANSIT-DIFFIMAGE package[31] by S. Bryson to calculate accurate centroids of the TCE and the assumed host star taking account of the pixel response function (PRF).

Finally, we eliminated secondary eclipses by matching them to the period and epoch of the star. We used the expected depth of the secondary eclipse as well as the phase offset from the known hot Jupiter transits and manually inspected each light curve to rule out that they could be planets at half or twice the hot Jupiter's orbital period.

The TCEs that passed all above vetting steps are the planet detections listed in Section 4. These detections are used as the numerator of the occurrence rate in Section 5.

3.3. Injection–Recovery Simulation

In order to evaluate the detection efficiency of the planet search pipeline described in Section 3.1 and the vetting procedures described in Section 3.2, we performed injection–recovery tests of simulated transit signals. For each host star in the hot Jupiter sample, five simulated signals were created via randomly drawn planetary parameters from the prior distributions,

$$R_{\rm p} \sim \mathcal{U}(0.5,\ 10)\ R_{\oplus}, \tag{3a}$$

$$\log P \sim \mathcal{U}(4\ \text{hr},\ 10\ \text{days}), \tag{3b}$$

$$b \sim \mathcal{U}(0,\ 1 + R_{\rm p}/R_{\star}), \tag{3c}$$

where $\mathcal{U}(a, b)$ is the uniform distribution on the interval $[a, b]$. To calculate $R_{\rm p}$ and b, stellar masses and radii were either taken from TICv8 when available or fixed to solar values otherwise.[32] All orbits were assumed to be circular, and we adopted a fixed linear limb-darkening law with coefficient 0.3. We calculated the simulated signals from these parameters using the limb-darkened transit light-curve model implemented by the BATMAN Python package, and the model was supersampled by a factor of 15, 5, and 2 for TESS sectors with FFI exposure times of 30 minutes, 10 minutes, and 200 s, respectively. Each simulated signal was injected into the corresponding hot Jupiter host star's TESS light curve, and we searched the resultant light curve using the same BLS transit search pipeline as in Section 3.1. As before, we used $\mathrm{S/N} > 7$ as the criterion for declaring a BLS signal to be a TCE.

[30] The original version is available on GitHub at https://github.com/nksaunders/giants.

[31] Available on GitHub at https://github.com/stevepur/transit-diffImage.

[32] Since the injection–recovery simulation is only used to derive an empirical relationship between theoretical transit S/N and pipeline detection efficiency, the exact choice of stellar parameters here has no bearing on the final occurrence rate as long as the range of S/N is sufficiently sampled. Rather, the choice of stellar parameters affects the final result through the assumed planet radius prior distribution in Equation (12b), where we *did* use the refined stellar parameters from Section 2.3 to derive the imputed transit depth of each simulated planet.

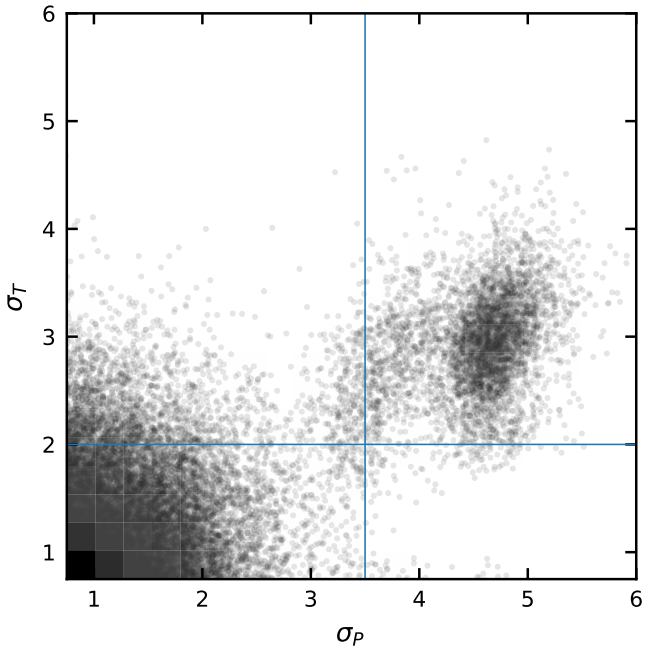


Figure 3. A scatter plot of σ_P versus σ_T for the detection of injected transit signals, similar to Figure 2 of J. L. Coughlin et al. (2014). The thin blue lines denote the chosen significance levels for ephemeris matching in Equation (4) and divide the plane into four quadrants. The cluster of points in the upper right quadrant corresponds to true ephemeris matches, while the points in the lower left are random false matches.

Rather than manually vetting the TCEs as in Section 3.2, we automatically matched the detected TCEs to the expected period and transit times using the ephemeris-matching method described by J. L. Coughlin et al. (2014). Using their definition, we set the criteria for ephemeris matching to be

$$\sigma_P > 3.5,\ \sigma_T > 2.0, \tag{4}$$

where P is the period, T is the transit time or epoch, and the σ values are converted from the fractional differences in P or T (J. L. Coughlin et al. 2014). Figure 3, emulating Figure 2 of J. L. Coughlin et al. (2014), confirms that the chosen significance levels in Equation (4) capture the mode of true ephemeris matches in the upper right while excluding the mode of random matches at low σ_P and σ_T values in the lower left. The number of matches as a fraction of injected signals is the empirical detection efficiency, which we denote ε, and we evaluate its dependence on the transit S/N in Section 3.4.

3.4. Transit Detection Efficiency

The injection–recovery simulation resulted in a map of sets of simulated planetary parameters to Boolean values indicating the success or failure of recovery. For the convenience of calculating the occurrence rate later in Section 5, we convert the injection–recovery results into an analytical formula that expresses the fraction of planets successfully detected by our search in terms of their transit signal's theoretical S/N.

We calculate a planet's theoretical transit S/N as

$$\mathrm{S/N} = \frac{\delta}{\sqrt{\sigma_{\rm sum}^2 P / T_{\rm dur}}}, \tag{5}$$

where δ is the transit depth, P is the orbital period, $T_{\rm dur}$ is the transit duration, and $\sigma_{\rm sum}^2$ is the "harmonic sum" of σ_i^2, the

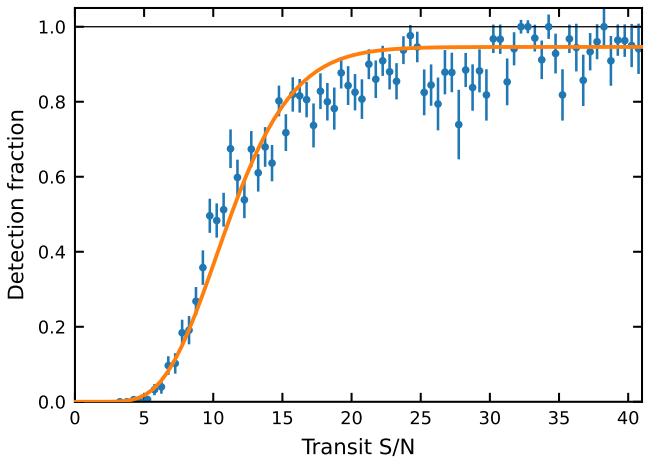


Figure 4. Detection fraction as a function of transit S/N. The blue marks are the recovery fraction of injected planets within each S/N bin, with error bars representing the Agresti–Coull confidence interval of binomial proportion, and the orange curve is a scaled gamma distribution CDF. The detection fraction asymptotically approaches ≈0.95 as the transit S/N → ∞.

squared uncertainty of the ith data point ($i = 1, 2, \ldots, N$):

$$\sigma^2_{\rm sum} = \left(\sum_{i=1}^{N} \frac{1}{\sigma_i^2}\right)^{-1}. \quad (6)$$

In the case where the data points have identical σ_i, this expression reduces to the familiar $\sigma^2_{\rm sum} = \sigma_i^2/N$.

In order to relate the theoretical S/N to the actual detection fraction, we empirically fitted the cumulative distribution function (CDF) of the gamma distribution with a shape parameter α, scale parameter θ, and maximum detection fraction C,

$$F(x;\, \alpha,\, \theta,\, C) = \frac{C}{\Gamma(\alpha)\, \theta^{\alpha}} \int_0^x t^{\alpha-1} e^{-t/\theta} dt, \quad (7)$$

as was used by J. L. Christiansen et al. (2015) for characterizing the transit signal recovery of the Kepler pipeline. To properly account for the statistics of the binned detection fraction, we used the Agresti–Coull interval (A. Agresti & B. Coull 1998), where the number of trials n and the success fraction p are modified into their estimators,

$$\hat{n} = n + 1,\, \hat{p} = \frac{1}{\hat{n}}\left(p + \frac{1}{2}\right), \quad (8)$$

which are used to calculate the interval

$$\sqrt{\frac{\hat{p}(1-\hat{p})}{\hat{n}}}. \quad (9)$$

We used the unmodified p for each S/N bin and the Agresti–Coull interval as the uncertainty in each bin.

We ended up with the best-fit parameters

$$\alpha = 9.21719769,\, \theta = 1.24222051,\, C = 0.94609528, \quad (10)$$

given to eight decimal places (understood as machine precision and not as significant figures). This scaled gamma CDF $F(x)$, illustrated in Figure 4, will be used in Section 5 to convert the theoretical transit S/N of the simulated planets into the expected pipeline detection efficiency ε by setting x = S/N.

4. Planet Detections

We detected the following inner companions, in ascending order of the orbital period of their respective hot Jupiters:

1. TOI-1408 c (J. Korth et al. 2024),
2. TOI-5143 b (S. N. Quinn et al. 2026),
3. TOI-1130 b (C. X. Huang et al. 2020a),
4. TOI-2494 b (S. N. Quinn et al. 2026),
5. WASP-84 c (G. Maciejewski et al. 2023), and
6. TOI-2000 b (L. Sha et al. 2023).

Of these, TOI-2000 b was discovered by an earlier version of the pipeline described in Section 3.1. These detections form the basis of the occurrence rate calculation in Section 5, and their system names are highlighted in magenta in Figure 1.

The following known nearby companions were not among those detected:

1. WASP-47 e and WASP-47 d, the inner and outer companions to WASP-47 b;
2. TOI-4468 c, the outer companion to TOI-4468 b (J. R. Livesey et al. 2026);
3. Kepler-730 c, the inner companion to Kepler-730 b; and
4. WASP-132 c, the inner companion to WASP-132 b.

The hot Jupiters WASP-47 b and TOI-4468 b were included in our sample, but their respective companions were not detected by the pipeline. The hot Jupiter Kepler-730 b was not a TOI and thus not in the sample. The hot Jupiter WASP-132 b was not in the sample because it lacked uncertainty for its radius in the TOI table on the ExoFOP website at the time of access. They will not count as detections for the purpose of the occurrence rate calculation.

5. Occurrence Rate of Nearby Companions to Hot Jupiters

Our goal is to estimate the occurrence rate η of nearby companions to hot Jupiters, conditioned on the hot Jupiter existing. To this end, we use a Bayesian statistical framework to calculate the posterior distribution of η given our sample of transiting companions to transiting hot Jupiters from TESS. We model each hot Jupiter observation as a Bernoulli trial where the probability of success is η. Then, given n such conditionally independent Bernoulli trials with s observed successes and a uniform prior for η, the posterior distribution of η can be modeled as the beta distribution Beta $(s + 1,\, n - s + 1)$, which is the conjugate prior of the binomial distribution. The probability density function (PDF) of η can be written as

$$f(\eta;\, s,\, n) = \frac{\eta^s (1-\eta)^{n-s}}{\mathrm{B}(s+1,\, n-s+1)}, \quad (11)$$

where B is the beta function. We take $s = 6$ as the number of hot Jupiters with detected companions (Section 4), while the number of trials n is the number of hot Jupiter systems searched corrected for observational completeness and accounting for the possibility of hot Jupiter false positives.

Observational completeness concerns two questions regarding a hypothetical companion to a hot Jupiter. First, given the orbital and planet parameters, does the companion transit? Second, if the companion transits, how likely is its detection? In order to evaluate these two questions for each hot Jupiter system, we simulate 10,000 hypothetical companions with the following procedure.

1. The companion's radius, orbital period, and mutual inclination with the hot Jupiter are drawn from a prior distribution.
2. The companion's impact parameter is calculated from the mutual inclination and the inclination of the hot Jupiter.
3. If the impact parameter indicates that the companion does not transit, the detection efficiency ε is set to 0, and we move on to the next simulated planet. Otherwise, we calculate the expected transit S/N and convert it into a predicted efficiency as $\varepsilon = F(\mathrm{S/N})$, with F being the empirically derived gamma CDF in Section 3.4.

Finally, we sum up the average detection efficiency of the simulated companions in each hot Jupiter system to arrive at an ESS of the hot Jupiters searched, which we take to be the number of trials n. The rest of this section describes each step in detail.

5.1. Prior Distribution of Nearby Companions

We draw the companion's radius R_p, orbital period P, and mutual inclination ψ from the following distributions:

$$R_\mathrm{p} \sim \mathcal{U}(1, 4)\, R_\oplus, \tag{12a}$$

$$P \sim \mathcal{U}(0.25, 10)\ \mathrm{days}, \tag{12b}$$

$$\psi \sim \mathrm{Rayleigh}(1\overset{\circ}{.}8), \tag{12c}$$

where $\mathcal{U}(a, b)$ is the uniform distribution on the interval $[a, b]$ and Rayleigh(σ) is the Rayleigh distribution with the scale parameter σ, subject to the condition

$$a/R_\star > 2. \tag{13}$$

For ease of comparison, we follow C. Huang et al. (2016) in setting σ to $1\overset{\circ}{.}8$ (converted to radians), a value that was in turn based on an estimate of $1\overset{\circ}{.}0$–$2\overset{\circ}{.}2$ for ψ in Kepler multitransiting systems by D. C. Fabrycky et al. (2014). We will explore how the inferred occurrence rate changes with the choice of prior distributions for ψ in Section 5.5.

5.2. Mutual Inclination and Impact Parameter

We calculate the impact parameter of the simulated companion from its ψ in order to find its transit duration, on which the transit S/N depends. We sample the companion's inclination i_2 through the relation

$$\cos i_2 = \cos i_1 \cos\psi + \cos B \sin i_1 \sin\psi, \tag{14}$$

where i_1 is the inclination of the hot Jupiter derived from its impact parameter (see Section 2.3) and B is an angle randomly drawn from $\mathcal{U}(0, 360^\circ)$.[33] The companion's impact parameter b_2 is then calculated from $\cos i_2$ assuming a circular orbit.

If $b_2 > 1 + R_\mathrm{p}/R_\star$, the planet is deemed not transiting, and its detection efficiency is set to 0. Otherwise, we proceed to calculate its transit S/N and detection efficiency as in Section 3.4 using the stellar radii from Section 2.3.

[33] If we set the orbital normal vector of the hot Jupiter as the z-axis, then ψ and B are, respectively, the polar and azimuthal angles of the companion's orbital normal vector.

5.3. Observational Completeness and Effective Sample Size

To calculate an ESS, we sum up the average detection efficiency ε of the simulated companions in each hot Jupiter system. In mathematical notation, the total ESS is

$$\mathrm{ESS} = \sum_{j=1}^{N_\mathrm{HJ}} \frac{1}{N_\mathrm{sim}} \sum_{i=1}^{N_\mathrm{sim}} \varepsilon_{ij}, \tag{15}$$

where ε_{ij} is the detection efficiency of the ith simulated companion of the jth hot Jupiter, $N_\mathrm{sim} = 10{,}000$ is the number of simulated companions per hot Jupiter, and N_HJ is the number of hot Jupiter systems in our sample. Figure 5 shows the average ε_{ij} in bins of planet period and radius expressed as percentages. Note that $\varepsilon_{ij} \equiv 0$ for nontransiting simulated companions, so the ESS is a measure of observational completeness taking account of both transit probability and pipeline detection efficiency.

Some of the hot Jupiter candidates in our sample from TESS surveys may still be false positives (e.g., background eclipsing binaries, hierarchical triples, blended foreground binaries). We multiply the above ESS = 92.50 by $(1 - \mathrm{FPR_{HJ}})$ from Section 2.2 to obtain the final $n = 86.95$, which is substituted into Equation (11) to obtain the posterior distribution PDF $f(\eta)$.

5.4. The Occurrence Rate

The PDF of the posterior distribution $f(\eta)$ of the occurrence rate η of nearby companions to hot Jupiters is shown in Figure 6. We quote the median and 90% credible interval of the occurrence rate as $(7.6^{+5.5}_{-3.8})\%$.

5.5. Dependence on Mutual Inclination

In order to test the effect of orbital alignment between the hot Jupiter and its nearby companion on the occurrence rate, we replace the Rayleigh distribution used in Section 5.1 with a series of 3D von Mises–Fisher (VMF) distributions of varying parameters. The 3D VMF distribution is the analog to the 2D normal distribution on the sphere, with a PDF over the unit vector $\hat{\mathbf{h}}$,

$$f(\hat{\mathbf{h}}; \hat{\mathbf{n}}, \kappa) = \frac{\kappa}{4\pi \sinh\kappa} \exp(\kappa \hat{\mathbf{n}} \cdot \hat{\mathbf{h}}), \tag{16}$$

with $\hat{\boldsymbol{n}}$ being a unit vector representing the reference direction and κ being a scale parameter characterizing the spread of the distribution. As such, if we take $\hat{\mathbf{n}}$ and $\hat{\mathbf{h}}$ to be the orbit normal vector of the hot Jupiter and its nearby companion, respectively, then the VMF distribution is a good candidate for parameterizing their degree of alignment via the scale parameter κ. If we marginalize this distribution over the azimuthal angle about $\hat{n}$, leaving only the mutual inclination ψ (with $\cos\psi = \hat{\mathbf{n}} \cdot \hat{\mathbf{h}}$), then we obtain the Fisher distribution with a PDF of

$$f(\psi; \kappa) = \frac{\kappa}{2 \sinh\kappa} e^{\kappa \cos\psi} \sin\psi, \tag{17}$$

which is the form often used in theoretical treatments of orbital alignment in multiplanet systems (e.g., D. C. Fabrycky & J. N. Winn 2009; J. C. Becker et al. 2017). The Fisher distribution with scale parameter κ reduces to Rayleigh($1/\sqrt{\kappa}$) for large κ

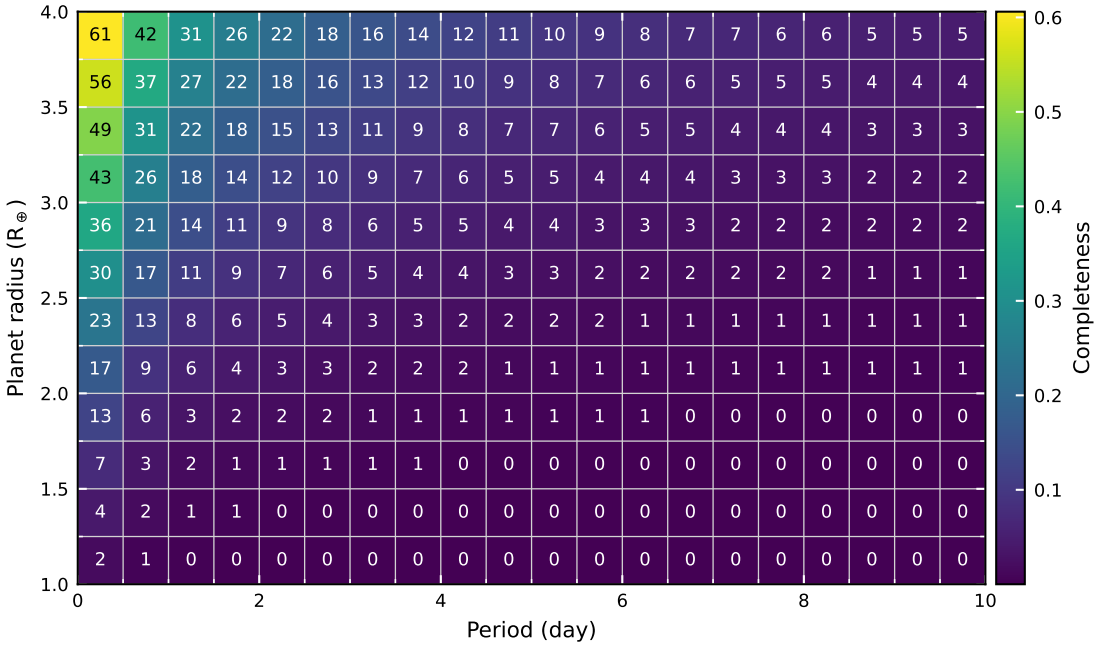


Figure 5. Overall observational completeness of simulated nearby companions to hot Jupiters in bins of the orbital periods and planet radii of the companions (Section 5.3), expressed as percentages. The observational completeness takes account of both transit probability and detection efficiency.

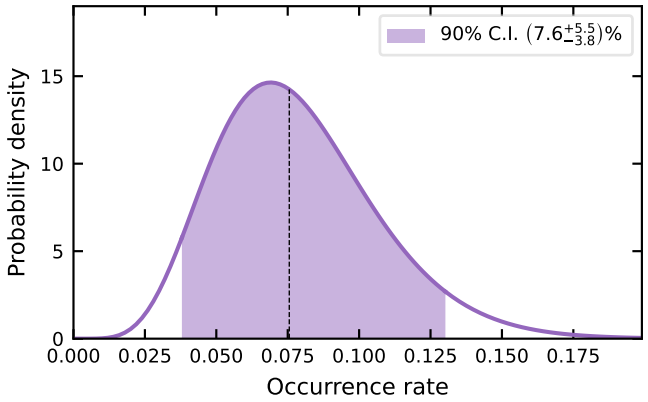


Figure 6. Posterior distribution of the occurrence rate of nearby companions (0.25 day $\leqslant P <$ 10 days, $1 \leqslant R_p/R_\oplus < 4$) to hot Jupiters. The 90% credible interval about the median is $(7.6^{+5.5}_{-3.8})$%, with the median indicated by a dashed vertical line and the interval shaded.

and small ψ and to an isotropic distribution (i.e., uniform in $\cos\psi$) as $\kappa \to 0$, representing the cases of good alignment versus maximal misalignment, respectively.

We find that as $\kappa \to 0$, we have $n \approx 17$, and as $\kappa \to \infty$, $n \approx 89$. This translates to an occurrence rate of (37^{+19}_{-17})% if the companion is isotropically distributed and $(7.4^{+5.4}_{-3.7})$% if the companion is aligned.

6. Discussion

In this work, we measure the occurrence rate of small (radius 1–4 $R_\oplus$) nearby (orbital period 0.25–10 days) companions to hot Jupiters to be $(7.6^{+5.5}_{-3.8})$%. In agreement with previous estimates of the occurrence rates of nearby companions (C. Huang et al. 2016; B. J. Hord et al. 2021), we find that hot Jupiters tend to be solitary. Historically, this fact has been taken as evidence that hot Jupiter formation is dynamically violent and tends to destabilize nearby planetary companions. In this section, we revisit these conclusions in light of our new results.

6.1. Comparison to Inner Companions of Small Short-period Planets

Do hot Jupiters have fewer nearby companions than the typical small short-period transiting planets, such as the ones observed by Kepler? Answering this question puts the loneliness of hot Jupiters into the broader context of planetary system architectures. Using data from Kepler DR25 (S. E. Thompson et al. 2018), we calculated the probability of a planetary system hosting small transiting short-period planets also hosting another transiting small planet nearby ($P <$ 10 days). Specifically, we selected small planets with

1. host star effective temperatures $T_{\rm eff,\star} > 4500$ K,
2. radii $R_p < 4\,R_\oplus$ (assuming Gaia DR2 stellar parameters),
3. periods 0.25 day $\leqslant P <$ 10 days, and
4. impact parameters $b < 0.9$.

We set an additional stellar effective temperature criterion to make sure the overall stellar sample is similar to that of hot Jupiter hosts. We found that this probability is 17.5% for the small planets even without correcting for completeness, much higher than the intrinsic occurrence rate for nearby companions to hot Jupiters.

We further estimated a preliminary intrinsic occurrence rate of these inner companions using the same prior distribution of planetary parameters for the companions of hot Jupiters described in Section 5.1. Combined with the detection completeness functions provided by the Kepler team (C. J. Burke et al. 2015; J. L. Christiansen et al. 2015), we find that, on average, the probability of a system hosting a short-period small planet also hosting another small planet within 10 days is (77 ± 5)%. We caution that these results are highly sensitive to the choice of prior distributions for the companion's period and radius, which is not taken into account in the uncertainties, although it would not change the

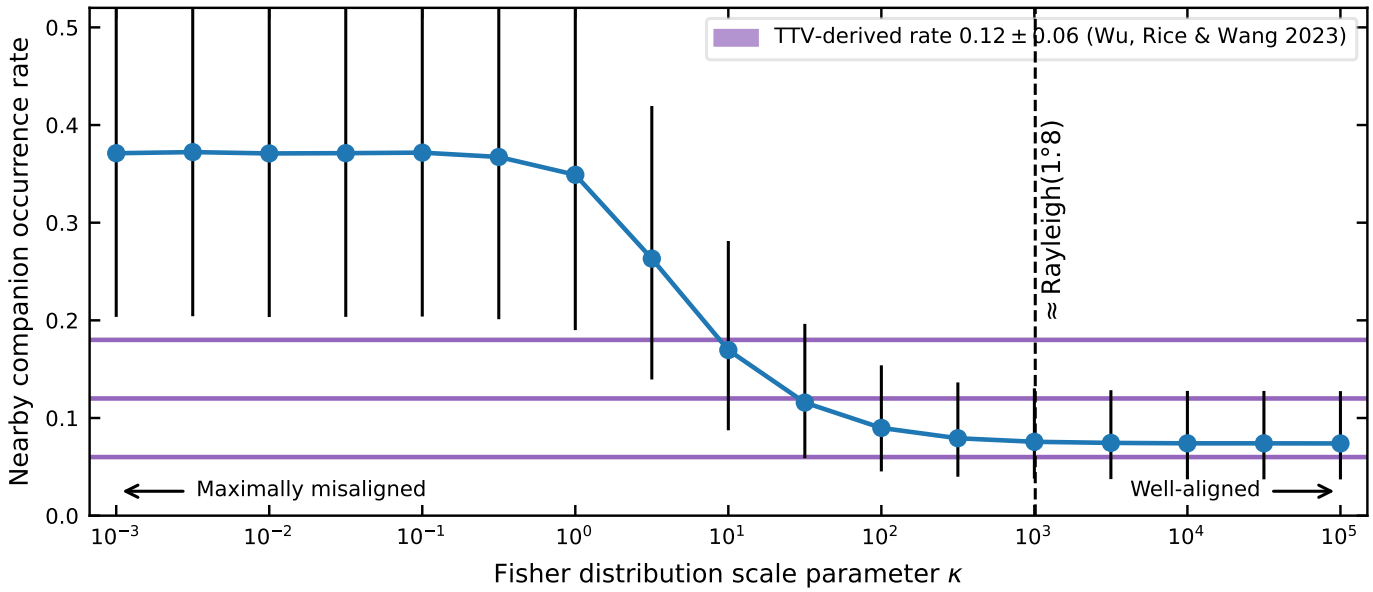


Figure 7. Occurrence rate of nearby companions (0.25 day $\leqslant P <$ 10 days, $1 \leqslant R_p/R_\oplus < 4$) to hot Jupiters as a function of their orbital alignment, parameterized as the scale parameter κ of a Fisher distribution prior on their mutual inclination. The posterior of each occurrence rate is a beta distribution, and we take the median and 90% interval as the marks and error bars shown. The vertical line ($\kappa \approx 10^3$) corresponds to the Rayleigh(1°.8) distribution, which is used as the mutual inclination prior to derive our main occurrence rate result of $(7.6^{+5.5}_{-3.8})\%$. For comparison, we shade the (12 ± 6)% credible interval of a similar occurrence rate derived from TTVs of hot Jupiters from the Kepler mission by D.-H. Wu et al. (2023). While their occurrence rate is not directly comparable to ours, reconciling the two different detection methods appears to rule out the case of maximal misalignment between hot Jupiters and their nearby companions.

conclusion that the probability of having a companion is significantly higher for small short-period planets compared to hot Jupiters.

6.2. Comparing to Occurrence Rate Obtained from Transit-timing Variation

Another important clue we can glean from our analysis is a constraint on the mutual inclination distribution for hot Jupiters and their close companions. The mutual inclination between a hot Jupiter and its nearby companion tells us a great deal about the formation and migration history of these systems. If the hot Jupiter and its nearby companion are well aligned, then it is evidence that the system had a relatively quiescent dynamical history. While we can directly constrain the sky-projected orbital orientation of the hot Jupiter through Rossiter–McLaughlin measurements (D. B. McLaughlin 1924; R. A. Rossiter 1924), it is challenging to achieve the S/N required for the small companion within its transit duration. Thus, we are unlikely to directly constrain the mutual inclination between the hot Jupiter and its nearby companion in the near future. The assumed mutual inclination distribution directly affects the occurrence rate we measure by altering the observational completeness of nearby companions, because they must transit in order to be detected in our search. Having explored how the degree of alignment between hot Jupiters and their nearby companions affects the calculated occurrence rate in Section 5.5, we now compare our result to occurrence rates derived from transit-timing variations (TTVs) of hot Jupiters, which can detect nontransiting companions by their gravitational influence on a hot Jupiter's orbit.

After a comprehensive search for TTVs among all hot Jupiters observed by Kepler, D.-H. Wu et al. (2023) found two TTV signals among 50 hot Jupiters in their sample, implying an occurrence rate of (12 ± 6)% for nearby companions to hot Jupiters, where "nearby" is defined as having a period ratio of ≈1.5–4. Their result is highlighted in Figure 7. Although their result is not directly comparable to ours due to differences in the assumption of priors for the underlying distribution of nearby companions and the different detection characteristics of TTV- and transit-based methods, reconciling the rates derived from the two methods appears to be incompatible with the case of maximal misalignment between hot Jupiters and their nearby companions (i.e., $\kappa \ll 1$). This would rule out unusual formation scenarios that result in the hot Jupiter and its companion being in nearly perpendicular orbits, as would be the case suggested by K. Batygin et al. (2016).

A more careful comparison between the TTV- and transit-based methods would require a joint search for TTVs and transits among a complete sample of well-characterized Kepler and TESS hot Jupiters. As a first step toward this process, we note that Z. Zhang et al. (2024) have performed a TTV search among 260 hot Jupiters from TESS, constraining the upper mass limit for potential companions to be several M_J. A future work could combine and extend the results from D.-H. Wu et al. (2023), Z. Zhang et al. (2024), and this work and invert the statistical framework used to derive occurrence rates to instead constrain the underlying distribution of mutual inclinations in systems hosting hot Jupiters with nearby companions.

6.3. Do Hot Jupiter Inner Companions Have a Small Preferential Misalignment?

We can also learn about the mutual inclination distribution of the hot Jupiters and their close neighbors by studying the impact parameter distributions of the systems in our sample. We note that among the nine hot Jupiters with *inner* companions, four of them (TOI-1408, TOI-5143, TOI-2494, and TOI-1130) have grazing transits (these systems are marked with an asterisk in Figure 1). Whether a single transiting planet is grazing depends only on the geometry of an observer

viewing a randomly oriented orbital plane. In a system of two transiting planets, however, the probability of either of the planets grazing also depends on their mutual inclination. If the two planets are perfectly aligned ($\psi = 0$), then the probability of finding a grazing planet is independent of the existence of the other transiting planet. But if the two planets are slightly misaligned, then the probability of finding one of the planets grazing given the presence of another transiting planet in the same system is boosted from what one might expect by random alignment. Here, we investigate whether finding four out of nine grazing hot Jupiters is more than what chance alignment can explain.

In order to calculate the grazing probability, we took the planet-to-stellar radius ratio of the ith hot Jupiter $k_i = R_{\mathrm{p},i}/R_{\star,i}$ and calculated the grazing probability p_i as

$$p_i = \frac{2k_i}{1 + k_i}. \tag{18}$$

Then, we averaged the grazing probability and used the average $p = (\sum_{i=1}^{9} p_i)/9$ as the parameter of a binomial distribution with the PDF

$$f_{\mathrm{binom}}(k; n, p) = \binom{n}{k} p^k (1 - p)^{n-k}, \tag{19}$$

where $n = 9$. Since the four planets are grazing, their radii are not known precisely, so we assume $R_{\mathrm{p}} = 1\,R_{\mathrm{J}}$. This gives an average grazing probability $p = 0.19$, which implies that the probability of having four or more grazing planets due to random viewing geometry is

$$\Pr(\geqslant 4\,\mathrm{grazing}) = \sum_{k=4}^{9} f_{\mathrm{binom}}(k; 9, 0.19) \approx 0.075. \tag{20}$$

This tantalizing statistical hint merits more investigation as we detect more systems in the future. If hot Jupiters with transiting inner companions are more likely to be grazing than we would expect from the random orientation of the viewing geometry alone, as would be the case for solitary hot Jupiters without nearby companions, then there may be a systematic small misalignment between these hot Jupiters and their inner companions. This misalignment could be the remnant dynamic signature of past migration.

6.4. Hot Jupiters with Inner Companions Also Have Cold Outer Companions

We can also investigate the systems with close companions and study their architectures beyond short-period transiting systems. Although transits are an effective way of finding additional planets in hot Jupiter systems, they may not give us the full picture of the architecture of these systems as transit probability falls off for longer orbital periods. Indeed, using up to 30 yr of RV measurements from the California Legacy Survey, J. K. Zink & A. W. Howard (2023) found that virtually all hot Jupiters have at least one more "cold" companion at much greater orbital periods. Since the very presence of these cold companions likely caused the hot Jupiters to migrate inward after disk dispersal, it would be instructive to look for cold companions in hot Jupiter systems with nearby companions to see whether they differ from the hot Jupiter population at large. Here, we assemble evidence from the literature for cold outer companions.

1. *WASP-47*. M. Neveu-VanMalle et al. (2016) found a cold companion, WASP-47 c, with orbital period $P = (588.8 \pm 2.0)$ days and minimum mass $M_{\mathrm{p}} \sin i = (398.9 \pm 9.1)\,M_{\oplus}$ (E. M. Bryant & D. Bayliss 2022). Additionally, WASP-47 d is a nearby outer companion (J. C. Becker et al. 2015).
2. *WASP-132*. Planet d is detected by RV with $P = (1811.8^{+42.6}_{-44.4})$ days, $M_{\mathrm{p}} \sin i = (5.29^{+0.48}_{-0.46})\,M_{\mathrm{J}}$ (N. Grieves et al. 2025). There is an additional linear trend in the RV (with a baseline of ≈9 yr implying $P \gtrsim 18$ yr) that may be a brown dwarf, in line with evidence for excess astrometric uncertainty in Gaia DR2 and DR3.
3. *TOI-1130*. There is an additional linear trend implying $P \gtrsim 160$ days (L. Borsato et al. 2024).
4. *TOI-1408*. There is an additional nonlinear trend implying $P \approx 2530$ days, $M \approx (14.6 \pm 0.3)\,M_{\mathrm{J}}$ (J. Korth et al. 2024).

In addition, TOI-2000 showed planet-sized RV signals at ≈17 and ≈90 days not explained by spectroscopic stellar activity indicators or photometric variations (L. Sha et al. 2023), although the RV baseline was too short to draw any conclusions at the time. Since then, the High Accuracy Radial velocity Planet Searcher (HARPS) spectrograph at the ESO La Silla 3.6 m telescope has made 39 additional RV measurements from 2023 December to 2024 March,[34] which showed an overall offset from the RVs 3 yr prior in 2021 at the 20 m s^{-1} level, although it is too early to say whether this offset is due to long-term stellar activity or an additional long-period planet.

Given that these systems are newly characterized and lack long-term RV monitoring, it is quite possible that there are cold outer companions in the remaining systems whose signals are hiding in plain sight, which would imply that hot Jupiters with nearby companions seem to also have cold companions at a rate comparable to that for other hot Jupiters in general estimated by J. K. Zink & A. W. Howard (2023). The presence of outer companions is believed to be a viable way to kick-start HEM, but if hot Jupiters with nearby companions, which presumably did not undergo HEM, also have a similar (or even greater) prevalence of outer companions, then the link between outer companions and HEM would be more complicated than it currently appears; namely, the mere presence of a cold companion is not sufficient to trigger HEM in producing a hot Jupiter. Continued long-term RV monitoring of these systems can potentially reveal this tension by comparing the mass and eccentricity of these suspected cold companions to the distribution of other hot Jupiters' cold companions.

6.5. Implications for Formation Theories

In summary, we find that about $(7.6^{+5.5}_{-3.8})\%$ of all hot Jupiters have closely orbiting companion planets, that the mutual inclination of these planets is small but nonzero and probably larger than the mutual inclination of small planet systems, and that the frequency of long-period outer companions seems similar to that of hot Jupiters without close companion planets. We draw the following conclusions about the formation of hot Jupiters.

1. At least $(7.6^{+5.5}_{-3.8})\%$ of hot Jupiters (i.e., the ones with nearby companions) must not form via HEM, which would almost certainly disrupt any nearby planetary

[34] ESO program 112.25WB; PI: Chelsea X. Huang.

companions. Moreover, the likely low mutual inclinations between hot Jupiters and their close companions also suggest relatively quiescent formation scenarios.

2. Moreover, since $(7.6^{+5.5}_{-3.8})\%$ is a strict lower limit on the fraction of systems that formed via dynamically quiescent mechanisms, the true fraction of hot Jupiters that form in this way could be larger. For example, simulations of hot Jupiters with nearby companions that formed via disk migration indicate that only about one-third of such close companions survive for long timescales (D.-H. Wu & Y. He 2023). This means that our result that $(7.6^{+5.5}_{-3.8})\%$ of hot Jupiters have close companions is consistent with a larger fraction ($\approx$20%) of hot Jupiter systems forming via disk migration.

Going forward, more detailed measurements and studies of the architectures of these systems, including the occurrence rate of specifically ultra-short-period planets (S. Wang et al. 2025), stellar obliquities and mutual inclinations (Y. He et al. 2024), and long-term RV surveys to measure the frequency of long-period massive planets (J. K. Zink & A. W. Howard 2023), will make it possible to estimate the relative importance of the different hot Jupiter formation channels.

7. Conclusions

Using 5 yr of TESS data, we have performed the most comprehensive search for nearby transiting companion planets to hot Jupiters to date. After accounting for observational completeness and pipeline detection efficiency, we arrived at an intrinsic occurrence rate of $(7.6^{+5.5}_{-3.8})\%$ for nearby companions to hot Jupiters. This result is highly sensitive to the assumed mutual inclination distribution between the hot Jupiters and their companions, and we instead have $(37^{+19}_{-17})\%$ for the case of maximal misalignment and $(7.4^{+5.4}_{-3.7})\%$ for the case of perfect alignment. Comparing our rate based on transit detections to that based on TTV detections appears to disfavor the case of maximal misalignment, but there may nevertheless be a preference for small misalignment as there is a hint that more hot Jupiters with nearby companions are grazing than can be explained by random viewing geometry. A review of RVs in the literature reveals that about half of the known hot Jupiters with nearby companions either have or are suspected to have cold companions, raising questions about the role cold companions play in triggering the formation of hot Jupiters via HEM. A future comprehensive search for nearby companions with transits, TTVs, and RVs may elucidate the underlying mutual inclination distribution. The picture is emerging that these nearby companions to hot Jupiters, while a relatively uncommon outcome of hot Jupiter formation, provide a key constraint on the relative frequency of each formation channel.

Acknowledgments

We thank Joshua N. Winn for suggestions that led to our implementation of Section 6.1.

Funding for the TESS mission is provided by NASA's Science Mission Directorate. We acknowledge the use of public TESS data from pipelines at the TESS Science Office and the TESS Science Processing Operations Center. This research has made use of the Exoplanet Follow-up Observation Program website (ExoFOP; NExScI 2022), which is operated by the California Institute of Technology, under contract with the National Aeronautics and Space Administration under the Exoplanet Exploration Program. This paper includes data collected by the TESS mission that are publicly available from the Mikulski Archive for Space Telescopes (MAST).

This work makes use of observations from the LCOGT network. Part of the LCOGT telescope time was granted by NOIRLab through the Mid-Scale Innovations Program (MSIP). MSIP is funded by NSF. This paper is based on observations made with the Las Cumbres Observatory's education network telescopes that were upgraded through generous support from the Gordon and Betty Moore Foundation.

This work is partly supported by JSPS KAKENHI grant Nos. JP24H00017, JP24K00689, JP24H00248, JP24K17082, and JP24K17083; JSPS grant-in-aid for JSPS Fellows grant Nos. JP24KJ0241 and JP25KJ0091; and JSPS Bilateral Program No. JPJSBP120249910. This paper is based on observations made with the MuSCAT instruments, developed by the Astrobiology Center (ABC) in Japan, the University of Tokyo, and Las Cumbres Observatory (LCOGT). This article is based on observations made with the MuSCAT2 instrument, developed by ABC, at Telescopio Carlos Sánchez, operated on the island of Tenerife by the IAC in the Spanish Observatorio del Teide. MuSCAT3 was developed with financial support by JSPS KAKENHI (JP18H05439) and JST PRESTO (JPMJPR1775) and is located at the Faulkes Telescope North on Maui, Hawaii (USA), operated by LCOGT. MuSCAT4 was developed with financial support provided by the Heising-Simons Foundation (grant 2022-3611), JST grant No. JPMJCR1761, and the ABC in Japan and is located at the Faulkes Telescope South at Siding Spring Observatory (Australia), operated by LCOGT.

Funding for K.B. was provided by the European Union (ERC AdG SUBSTELLAR, GA 101054354).

A.B. acknowledges the support of the M.V. Lomonosov Moscow State University Program of Development.

Z.L.D. would like to thank the generous support of the MIT Presidential Fellowship and the MIT Collamore–Rogers Fellowship and to acknowledge that this material is based upon work supported by the National Science Foundation Graduate Research Fellowship under grant No. 1745302.

K.A.C. acknowledges support from the TESS mission via subaward s3449 from MIT.

T.G. acknowledges that ASTEP benefited from the support of the French and Italian polar agencies IPEV and PNRA in the framework of the Concordia station program and from OCA, INSU, Idex UCAJEDI (ANR-15-IDEX-01), ESA through the Science Faculty of the European Space Research and Technology Centre (ESTEC), the European Research Council (ERC) under the European Union's Horizon 2020 research and innovation program (grant agreement No. 803193/BEBOP), and the Science and Technology Facilities Council (STFC; grant Nos. ST/S00193X/1, ST/W002582/1, and ST/Y001710/1).

F.M. acknowledges the financial support from the Agencia Estatal de Investigación del Ministerio de Ciencia, Innovación y Universidades (MCIU/AEI) through grant PID2023-152906NA-I00.

E.P. acknowledges financial support from the Agencia Estatal de Investigación of the Ministerio de Ciencia e Innovación MCIN/AEI/10.13039/501100011033 and the ERDF "A way of making Europe" through project PID2021-

125627OB-C32 and from the Centre of Excellence "Severo Ochoa" award to the Instituto de Astrofisica de Canarias.

Software: Astropy (Astropy Collaboration et al. 2013, 2018, 2022), MIT Quick Look Pipeline (QLP) (C. X. Huang 2020; C. X. Huang et al. 2020b, 2020c; M. Kunimoto et al. 2021, 2022b), giants (N. Saunders et al. 2022), tess-diffImage, Pandas.

Facilities: Gaia, TESS.

ORCID iDs

Lizhou Sha https://orcid.org/0000-0001-5401-8079
Andrew M. Vanderburg https://orcid.org/0000-0001-7246-5438
Chelsea X. Huang https://orcid.org/0000-0003-0918-7484
Samuel Christian https://orcid.org/0000-0003-0046-2494
Kevin Burdge https://orcid.org/0000-0002-7226-836X
Nicholas Saunders https://orcid.org/0000-0003-2657-3889
Khalid Barkaoui https://orcid.org/0000-0003-1464-9276
Alexander Belinski https://orcid.org/0000-0003-3469-0989
Serge Bergeron https://orcid.org/0000-0003-0846-1744
Zoë L. de Beurs https://orcid.org/0000-0002-7564-6047
Allyson Bieryla https://orcid.org/0000-0001-6637-5401
Karen A. Collins https://orcid.org/0000-0001-6588-9574
Giuseppe Conzo https://orcid.org/0000-0002-2412-1558
Gareb Fernández-Rodríguez https://orcid.org/0000-0003-0597-7809
Akihiko Fukui https://orcid.org/0000-0002-4909-5763
Davide Gandolfi https://orcid.org/0000-0001-8627-9628
Tristan Guillot https://orcid.org/0000-0002-7188-8428
Joel D. Hartman https://orcid.org/0000-0001-8732-6166
Kai Ikuta https://orcid.org/0000-0002-5978-057X
David W. Latham https://orcid.org/0000-0001-9911-7388
Jerome P. de Leon https://orcid.org/0000-0002-6424-3410
Bob Massey https://orcid.org/0000-0001-8879-7138
Gabriel Murawski https://orcid.org/0000-0001-7809-1457
Felipe Murgas https://orcid.org/0000-0001-9087-1245
Norio Narita https://orcid.org/0000-0001-8511-2981
Mohammad Odeh https://orcid.org/0000-0002-8986-6681
Enric Palle https://orcid.org/0000-0003-0987-1593
Hannu Parviainen https://orcid.org/0000-0001-5519-1391
Gabrielle Ross https://orcid.org/0009-0006-7023-1199
Richard P. Schwarz https://orcid.org/0000-0001-8227-1020
Chris Stockdale https://orcid.org/0000-0003-2163-1437
Samuel N. Quinn https://orcid.org/0000-0002-8964-8377
Ian A. Waite https://orcid.org/0000-0002-3249-3538
Francis P. Wilkin https://orcid.org/0000-0003-2127-8952
George Zhou https://orcid.org/0000-0002-4891-3517

References

Agresti, A., & Coull, B. 1998, AmSta, 52, 119
Astropy Collaboration, Price-Whelan, A. M., Lim, P. L., et al. 2022, ApJ, 935, 167
Astropy Collaboration, Price-Whelan, A. M., Sipőcz, B. M., et al. 2018, AJ, 156, 123
Astropy Collaboration, Robitaille, T. P., Tollerud, E. J., et al. 2013, A&A, 558, A33
Batygin, K., Bodenheimer, P. H., & Laughlin, G. P. 2016, ApJ, 829, 114
Becker, J. C., Vanderburg, A., Adams, F. C., Khain, T., & Bryan, M. 2017, AJ, 154, 230
Becker, J. C., Vanderburg, A., Adams, F. C., Rappaport, S. A., & Schwengeler, H. M. 2015, ApJL, 812, L18
Beleznay, M., & Kunimoto, M. 2022, MNRAS, 516, 75
Borsato, L., Degen, D., Leleu, A., et al. 2024, A&A, 689, A52
Bryant, E. M., & Bayliss, D. 2022, AJ, 163, 197
Burke, C. J., Christiansen, J. L., Mullally, F., et al. 2015, ApJ, 809, 8
Cañas, C. I., Wang, S., Mahadevan, S., et al. 2019, ApJL, 870, L17
Choi, J., Dotter, A., Conroy, C., et al. 2016, ApJ, 823, 102
Christiansen, J. L., Clarke, B. D., Burke, C. J., et al. 2015, ApJ, 810, 95
Coughlin, J. L., Thompson, S. E., Bryson, S. T., et al. 2014, AJ, 147, 119
Dotter, A. 2016, ApJS, 222, 8
Fabrycky, D. C., Lissauer, J. J., Ragozzine, D., et al. 2014, ApJ, 790, 146
Fabrycky, D. C., & Winn, J. N. 2009, ApJ, 696, 1230
Fausnaugh, M. M., Burke, C. J., Ricker, G. R., & Vanderspek, R. 2020, RNAAS, 4, 251
Grieves, N., Bouchy, F., Armstrong, D. J., et al. 2025, A&A, 693, A144
Guerrero, N. M., Seager, S., Huang, C. X., et al. 2021, ApJS, 254, 39
Hartman, J. D., & Bakos, G. A. 2016, A&C, 17, 1
He, Y., Wu, D.-H., & Jin, S. 2024, MNRAS, 530, 3934
Hoffman, J. 2022, Cuvarbase: Fast Period Finding Utilities for GPUs, Astrophysics Source Code Library, ascl:2210.030
Hord, B. J., Colón, K. D., Berger, T. A., et al. 2022, AJ, 164, 13
Hord, B. J., Colón, K. D., Kostov, V., et al. 2021, AJ, 162, 263
Huang, C., Wu, Y., & Triaud, A. H. M. J. 2016, ApJ, 825, 98
Huang, C. X. 2020, TESS Lightcurves From The MIT Quick-Look Pipeline (STScI/MAST)
Huang, C. X., Quinn, S. N., Vanderburg, A., et al. 2020a, ApJL, 892, L7
Huang, C. X., Vanderburg, A., Pál, A., et al. 2020b, RNAAS, 4, 204
Huang, C. X., Vanderburg, A., Pál, A., et al. 2020c, RNAAS, 4, 206
Korth, J., Chaturvedi, P., Parviainen, H., et al. 2024, ApJL, 971, L28
Kovács, G., Zucker, S., & Mazeh, T. 2002, A&A, 391, 369
Kunimoto, M., Huang, C., Tey, E., et al. 2021, RNAAS, 5, 234
Kunimoto, M., Tey, E., Fong, W., Hesse, K., & Shporer, A. 2022a, RNAAS, 6, 235
Kunimoto, M., Tey, E., Fong, W., et al. 2022b, RNAAS, 6, 236
Kunimoto, M., Tey, E., Fong, W., et al. 2023, RNAAS, 7, 28
Latham, D. W., Rowe, J. F., Quinn, S. N., et al. 2011, ApJL, 732, L24
Lin, D. N. C., Bodenheimer, P., & Richardson, D. C. 1996, Natur, 380, 606
Livesey, J. R., Hord, B. J., Becker, J., et al. 2026, ApJL, submitted
Maciejewski, G., Golonka, J., Loboda, W., et al. 2023, MNRAS, 525, L43
Mayor, M., & Queloz, D. 1995, Natur, 378, 355
McKee, B. J., Montet, B. T., Yee, S. W., et al. 2025, ApJ, 981, 106
McLaughlin, D. B. 1924, ApJ, 60, 22
Miller-Ricci, E., Rowe, J. F., Sasselov, D., et al. 2008, ApJ, 682, 593
Morton, T. D. 2015, isochrones: Stellar Model Grid Package, Astrophysics Source Code Library, ascl:1503.010
Mustill, A. J., Davies, M. B., & Johansen, A. 2015, ApJ, 808, 14
Neveu-VanMalle, M., Queloz, D., Anderson, D. R., et al. 2016, A&A, 586, A93
NExScI 2022, Exoplanet Follow-up Observing Program Web Service (IPAC)
Pollack, J. B., Hubickyj, O., Bodenheimer, P., et al. 1996, Icar, 124, 62
Quinn, S. N., Rodriguez, J. E., Collins, K. A., et al. 2026, AJ, 171, 359
Rasio, F. A., & Ford, E. B. 1996, Sci, 274, 954
Rodriguez, J. E., Quinn, S. N., Vanderburg, A., et al. 2023, MNRAS, 521, 2765
Rodriguez, J. E., Quinn, S. N., Zhou, G., et al. 2021, AJ, 161, 194
Rossiter, R. A. 1924, ApJ, 60, 15
Saunders, N., Grunblatt, S. K., Huber, D., et al. 2022, AJ, 163, 53
Schulte, J., Rodriguez, J. E., Bieryla, A., et al. 2024, AJ, 168, 32
Sha, L., Vanderburg, A. M., Huang, C. X., et al. 2023, MNRAS, 524, 1113
Shallue, C. J., & Vanderburg, A. 2018, AJ, 155, 94
Stassun, K. G., Oelkers, R. J., Paegert, M., et al. 2019, AJ, 158, 138
Stassun, K. G., Oelkers, R. J., Pepper, J., et al. 2018, AJ, 156, 102
Steffen, J. H., Ragozzine, D., Fabrycky, D. C., et al. 2012, PNAS, 109, 7982
Thompson, S. E., Coughlin, J. L., Hoffman, K., et al. 2018, ApJS, 235, 38
Vanderburg, A., Huang, C. X., Rodriguez, J. E., et al. 2019, ApJL, 881, L19
Vanderburg, A., & Johnson, J. A. 2014, PASP, 126, 948
Vanderburg, A., Latham, D. W., Buchhave, L. A., et al. 2016, ApJS, 222, 14
Wang, S., Pan, M., Dong, Y., Zhao, G., & Ji, J. 2025, ApJL, 982, L15
Wright, J. T., Marcy, G. W., Howard, A. W., et al. 2012, ApJ, 753, 160
Wu, D.-H., & He, Y. 2023, AJ, 166, 267
Wu, D.-H., Rice, M., & Wang, S. 2023, AJ, 165, 171
Yee, S. W., & Winn, J. N. 2023, ApJL, 949, L21
Yee, S. W., Winn, J. N., & Hartman, J. D. 2021, AJ, 162, 240
Yee, S. W., Winn, J. N., Hartman, J. D., et al. 2022, AJ, 164, 70
Yee, S. W., Winn, J. N., Hartman, J. D., et al. 2023, ApJS, 265, 1
Zhang, Z., Wang, W., Ma, X., et al. 2024, ApJS, 275, 32
Zhou, G., Huang, C. X., Bakos, G. Á., et al. 2019, AJ, 158, 141
Zhu, W., Dai, F., & Masuda, K. 2018, RNAAS, 2, 160
Zhu, W., & Dong, S. 2021, ARA&A, 59, 291
Zink, J. K., & Howard, A. W. 2023, ApJL, 956, L29